

# Performance and energy costs associated with scaling infrared heater arrays for warming field plots from 1 to 100 m

Bruce A. Kimball · Matthew M. Conley · Keith F. Lewin

Received: 28 March 2011 / Accepted: 25 August 2011 / Published online: 1 October 2011  
© Springer-Verlag (outside the USA) 2011

**Abstract** To study the likely effects of global warming on open-field vegetation, hexagonal arrays of infrared heaters are currently being used for low-stature (<1 m) plants in small ( $\leq 3$  m) plots. To address larger ecosystem scales, herein we show that excellent uniformity of the warming can be achieved using nested hexagonal and rectangular arrays. Energy costs depend on the overall efficiency (useable infrared energy on the plot per electrical energy in), which varies with the radiometric efficiency (infrared radiation out per electrical energy in) of the individual heaters and with the geometric efficiency (fraction of thermal radiation that falls on useable plot area) associated with the arrangement of the heaters in an array. Overall efficiency would be about 26% at  $4 \text{ ms}^{-1}$  wind speed for a single hexagonal array over a 3-m-diameter plot and 67% for a 199-hexagon honeycomb array over a 100-m-diameter plot, thereby resulting in an economy of scale.

## 1 Introduction

As atmospheric  $\text{CO}_2$  concentrations continue to rise and Earth's climate continues to warm, experiments with elevated levels of  $\text{CO}_2$  and temperature are needed to investigate the likely effects of global climate change on

ecosystems (e.g., Ainsworth et al. 2008). In order to have confidence that the experiments are as representative as possible of future conditions, it is desirable that many be conducted under free-air, open-field conditions, i.e.,  $\text{CO}_2$ - and temperature-free-air-controlled enhancement (T-FACE) experiments.

Techniques for free-air  $\text{CO}_2$  enrichment have been relatively well developed (e.g., Hendrey 1993; Okada et al. 2001; Miglietta et al. 2001; Lewin et al. 2009) compared to those for warming. Several techniques have been developed to warm plots of vegetation under open-field conditions (e.g., Harte et al. 1995; Nijs et al. 1996; Kimball 2005, 2011; and several references cited therein), but all have problems. One technique which shows promise is to utilize arrays of infrared heaters deployed in a hexagonal or other configuration so as to produce a uniform distribution of the thermal radiation across the plot (Kimball et al. 2008, in preparation; Luo et al. 2010; Wall et al. 2011). Having a uniform warming treatment across the whole plot area is essential in order to assure that any particular sample received the same warming treatment as other samples taken from elsewhere in the plot.

While having good uniformity of the warming treatment is essential, it is also desirable that the infrared heater arrays be efficient so that as much of the electrical power supplied to the arrays as possible results in thermal radiation impinging on the plants and any exposed soil within the plot area, thereby reducing the energy cost of conducting the experiments. Kimball (2005) presented a theory from which the efficiency of the heaters themselves could be calculated from a characteristic length of the radiating surface and wind speed. Herein, we will refer to this as the “radiometric efficiency,” which is the percentage of the electrical power supplied to the heaters that results in thermal radiation emitted by the heaters rather than lost by

---

B. A. Kimball (✉) · M. M. Conley  
U.S. Arid Land Agricultural Research Center,  
Agricultural Research Service, USDA,  
21881 North Cardon Lane,  
Maricopa, AZ 85238, USA  
e-mail: Bruce.Kimball@ars.usda.gov

K. F. Lewin  
Brookhaven National Laboratory,  
Upton,  
Long Island, NY 11973, USA

forced convection to the wind or natural convection from buoyant air currents. At the same time, it is desired, as much as possible, that the thermal radiation emitted by the infrared heaters impinge on the vegetation and exposed soil surfaces within the defined plot area, rather than being lost outside the plot. We define this “geometric efficiency” as the percentage of the thermal radiation emitted by the heaters that impinges on the plot area, and we will present theory to calculate this geometric efficiency. The “overall efficiency” is the percentage of electrical power supplied to the heaters that results in useful thermal radiation impinging on the plants and exposed soil within the plot area, and it is the product of the radiometric and geometric efficiencies.

Another obvious constraint is that the heaters themselves and their support hardware should not shade the plants from solar radiation. Zero shading is not possible, so what is an acceptable amount? The amount that is acceptable depends on the comfort level of the experimenters and of reviewers of resultant papers. To us, 10% shading seems an acceptable upper limit. Whatever the acceptable shading amount, it is always good experimental technique for the control or reference plots to be as similar as possible to the treated plots without the actual treatment, which in this application means that the reference plots should have dummy, non-functional heater arrays and support structures that mimic those used in the warmed plots.

The size of the infrared heater arrays needed to warm open-field ecosystem plots depends greatly on the stature of the experimental vegetation, which ranges from mown urban lawns (e.g., Bijoor et al. 2008) to tall trees (e.g., Körner et al. 2005). So far, only small stature (<1 m) vegetation has been investigated using infrared heating in small plots (<5 m diameter), but the need exists to provide warming treatments across much larger plots (Ainsworth et al. 2008), which additionally would allow studies on larger stature vegetation. Therefore, it is the objective of this paper to present thermal radiation distributions, efficiencies, operating costs, and solar shadings of various designs of infrared heater arrays over plot scales ranging from 1 to 100 m.

## 2 Thermal radiation distribution uniformity

### 2.1 Derivation of a theoretical equation to compute thermal radiation distribution

The warming pattern under a Kalgo heater (Table 1) was presented by Kimball (2005), with and without the reflector modification introduced by Harte et al. (1995). Patterns of warming and of actual down-welling thermal radiation were measured and presented by Kimball et al. (2008) for a nadir-pointed Mor-FTE heater (Table 1) and for hexagonal

arrays of such heaters tilted at 45° toward the center of field plots. However, because the number of possible configurations of various heater arrays with many heaters at varying tilts and heights is vast, it is desirable to have a method to predict the thermal radiation distribution pattern without having to actually construct each array and subsequently measure the resultant pattern. Here we present such a theoretical method to predict the distribution pattern from infrared heater arrays.

Many texts on the topic of heat transfer present theory on the exchange of thermal radiation between uniform black body surfaces (e.g., Gebhart 1961; Howell 2001). They show that the radiant emission from a surface,  $A_1$ , which goes directly to another surface,  $A_2$ ,  $q_{1-2}$  ( $W$ ) is:

$$q_{1-2} = F_{12}W_1A_1 \quad (1)$$

where  $W_1$  is the emissive power ( $W\ m^{-2}$ ) of surface 1,  $A_1$  is its area ( $m^2$ ), and  $F_{12}$  is an angle or view factor that is dimensionless and depends solely on the geometrical orientation of the two surfaces with respect to each other. In general, the angle factor from an elemental area of surface 1 to an elemental area of surface 2 is:

$$dF_{1-2} = (\cos \Theta_1 \cos \Theta_2) (\pi S^2)^{-1} dA_2 \quad (2)$$

where  $S$  is the length of the line from the surface 1 element to the surface 2 element,  $\Theta_1$  is the angle between  $S$  and the normal to surface 1,  $\Theta_2$  is the angle between  $S$  and the normal to surface 2, and  $dA_2$  is the area of the element of surface 2 (e.g., Gebhart 1961; Howell 2001). For many important common surfaces, such as the radiant transfer of energy from one wall of a rectangular room to another, Eq. 2 has been integrated, and graphs and catalogs of angle factors exist (e.g., Gebhart 1961; Howell 2001).

Graphs and catalogs suitable for determining the optimal height and orientation of infrared heaters to warm ecosystem field plots are not readily available, but they can be derived. Referring to Fig. 1, a black body heater element (surface 1) is deployed over a horizontal field plot element (surface 2). The  $x, y$  coordinates are  $x_h, y_h$  and  $x_p, y_p$  for the heater and plot elements, respectively. The heater is at a height of  $z_h$  above the plane of the plot, which is also the length of the vertical normal line,  $n_p$ , for the plot element. The plane of the plot is the top of the vegetative canopy (or bare soil or snow), and all the vertical distances are measured from the top of the canopy. The heater is tilted at angle  $\tau$  from vertical, and it is pointed at an angle  $\alpha$  from the  $x$ -axis. In order to utilize Eq. 2, expressions are needed for  $S$ ,  $\cos \Theta_h$ , and  $\cos \Theta_p$ , where  $S$  is the line from the heater to the plot element,  $\Theta_h$  is the angle between  $S$  and the normal to the heater surface,  $n_h$ , and  $\Theta_p$  is the angle between  $S$  and the normal to the plot element,  $n_p$ .



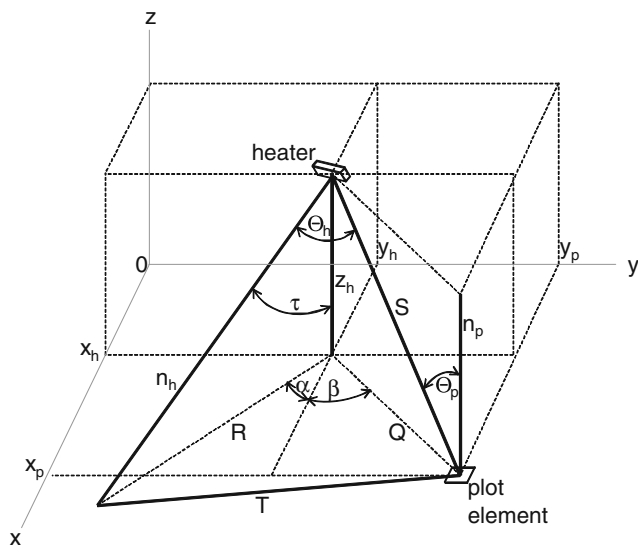


**Fig. 1** Diagram of the geometry between a black body infrared heater element and a horizontal plot element. The heater is at a height of  $z_h$  above plot surface, tilted by angle  $\tau$  from vertical, and turned by azimuth angle  $\alpha$  from the  $x$ -axis

Referring to Fig. 1 and utilizing the Pythagorean Theorem,

$$Q = [(y_p - y_h)^2 + (x_p - x_h)^2]^{1/2} \tag{3}$$

$$S = (Q^2 + z_h^2)^{1/2} \tag{4}$$

$$\cos \theta_p = z_h S^{-1} \tag{5}$$

Thus, two of the three factors needed for Eq. 2 can be easily obtained. However, obtaining  $\cos \theta_h$  requires more effort. Again referring to Fig. 1,

$$R = z_h \tan \tau \tag{6}$$

Utilizing the trigonometric identity that  $a^2 = b^2 + c^2 - 2bc \cos A$  where  $a$ ,  $b$ , and  $c$  are the sides of a triangle and  $A$  is the angle opposite side  $a$ ,

$$T^2 = Q^2 + R^2 - 2QR \cos (\alpha + \beta) \tag{7}$$

which can be written as:

$$T^2 = Q^2 + R^2 - 2QR (\cos \alpha \cos \beta - \sin \alpha \sin \beta) \tag{8}$$

where:

$$\cos \beta = (x_p - x_h) Q^{-1} \tag{9}$$

and

$$\sin \beta = (y_p - y_h) Q^{-1} \tag{10}$$

Finally, utilizing the same identity,

$$\cos \theta_h = (S^2 + n_h^2 - T^2) (2Sn_h)^{-1} \tag{11}$$

where:

$$n_h = z_h (\cos \tau)^{-1} \tag{12}$$

Therefore, the angle factor from the heater element to the plot element can be computed from:

$$dF_{h-p} = (\cos \theta_h \cos \theta_p) (\pi S^2)^{-1} dA_p \tag{13}$$

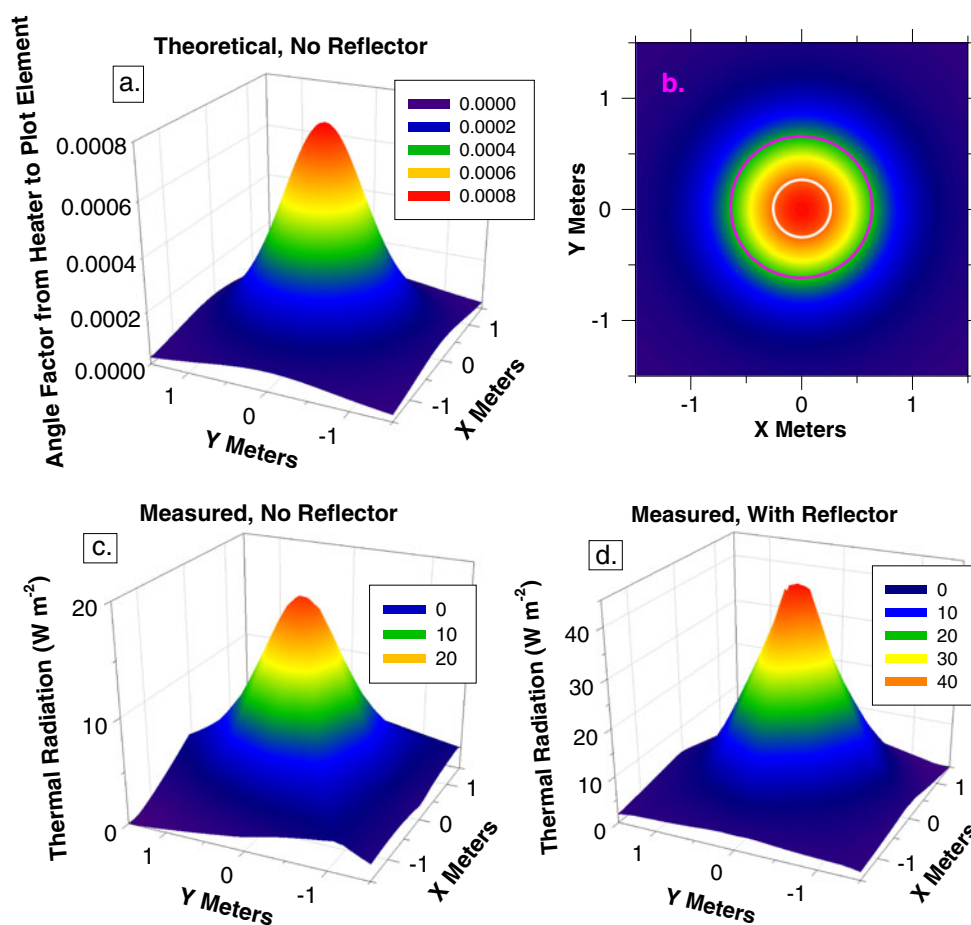
To utilize Eq. 13 to compute the total angle factor from heater to plot,  $F_{h-p}$ , the plot area is subdivided into many elements of area  $dA_p$ . If the size of the heater is small compared to the height of the heater,  $z_h$ , then the energy of the heater can be assumed to come from a single heater element. For this case,  $F_{h-p}$  is simply the sum of all the  $dF_{h-p}$  computed with Eq. 13 for every plot element from the single heater element. However, if the heater area is too large to be a single element, then the procedure has to be repeated for the several heater elements, and these values need to be accumulated into an overall sum. Similarly, if there is more than one heater in an array above the plot, then for each plot element, the sum of the  $dF_{h-p}$  from all the heaters is calculated.

### 2.2 Single heater pointed down (1 m scale)

The theoretical distribution of down-welling thermal radiation from a single small heater (similar to a Mor-ESES, Table 1) deployed 1 m above a field plot is decidedly conical (Fig. 2a, b). Therefore, the plot area over which the thermal radiation is uniform is rather small. If the plot diameter is defined as 0.56 m (Fig. 2b), such as done by Bijoor et al. (2008), then the relative range [(maximum–minimum)/mean] and CV (coefficient of variation) of the flux are excellent at 14.1% and 4.3%, respectively (Table 2). On the other hand, if the plot boundary is defined as 1.2 m (Fig. 2b), such as done by Hovenden et al. (2006), then the range and CV become very large, 193% and 48%, respectively.

To assure that Eq. 13 was indeed accurate for computing the distribution of radiation from real heaters, we measured the down-welling thermal radiation from a single 150-W Mor-ESES infrared heater on a plane 1.0 m below the heater indoors following Kimball et al. (2008) both with and without a 0.245-m-diameter reflector housing. Whether the reflector was present (Fig. 2d) or not (Fig. 2c), the distribution was markedly conical, just like the theoretical angle factors (Fig. 2a). With no reflector, the range and CV over a 0.56-m plot were 16% and 5% of the mean, respectively, which are close to the theoretical values. Over a 1.2-m plot, they were 62% and 17%, which is better than the theoretical values, but sampling would still be problematic. With the reflector in place, as would normally be the case, the range and CV over a 0.56-m plot were 31% and 7% and over a 1.2-m plot were 80% and 20%, respectively. Thus, compared to the theoretical case, the reflector improved the distribution

**Fig. 2** **a** Color-coded, 3D depiction of the theoretical angle factors for down-welling thermal radiation from a single infrared heater (like a Mor ESES, Table 1) deployed at a height of 1 m above a field plot. **b** Color-coded contour plot of the pattern from the heater in (a). The *white ring* indicates a 0.56-m-diameter plot boundary (e.g., Bijoer et al. 2008) and the *pink ring* indicates an equivalent 1.20-m-diameter boundary (e.g., Hovenden et al. 2006). **c** Color-coded, 3D plot of the measured down-welling thermal radiation from a bare 150-W Mor-ESES infrared heater (Table 1) on a plane 1.0 m below the heater. **d** The same as c for the same heater but with 0.254-m-diameter reflector housing installed



for the larger 1.2-m plot area but made it slightly worse for the 0.56-m area. In spite of the improvement over the 1.2-m area, the variation in radiation was still very large, so attempting to sample plants that received the same treatment would be problematic. What the reflector did accomplish, however, is a doubling of efficiency such that the radiation emitted from the back (upward) side of the heater was reflected back down to the plot area. Note that the scale of Fig. 2d is more than double that of Fig. 2c. For 150 W of electrical energy input, summing the radiation over the 0.56- and 1.2-m plot areas showed the efficiencies to be 3% and 11%, respectively, when no reflector was present. These values improved to 7% and 23%, respectively, when the reflector was in place.

### 2.3 Single-hexagon array of six heaters tilted 45° (3–5 m scale)

Kimball et al. (2008) deployed hexagonal arrays of small heaters (Mor-FTE, Table 1) over 3-m-diameter plots (7.1 m<sup>2</sup>) at a height of 1.2 m (0.4 times the plot diameter) above the vegetation and tilted 45° toward the center of the plot. They measured good uniformity of the down-welling

thermal radiation across the plot (range and CV of 55.8% and 12.0%, respectively). Kimball and Conley (2009) proportionally scaled up the hexagonal array to a diameter of 5 m (19.6 m<sup>2</sup>), and good uniformity was again measured (CV of 11%). Using Eq. 13, we calculated the theoretical distribution of the down-welling thermal radiation from such hexagonal arrays (Figs. 3a, b, 4). With a range and CV across the plot of 30.3% and 7.5%, respectively (Figs. 3a, b; Table 2), the theoretical distribution is somewhat more uniform than the measured data.

### 2.4 Seven-hexagon array with 24 nodes (8-m scale)

As discussed in the introduction, there is a need to extend the size of ecosystem plots. If very large infrared heaters were available, six such heaters could be deployed at a height of 0.4 times the diameter of the larger plot, and the theoretical distribution pattern of the radiation would be the same as depicted in Fig. 3a and b. However, huge infrared heaters are not commercially available, and a significant portion of the radiation of the heaters falls outside the useable plot area. Therefore, it becomes advantageous to deploy some of the heaters over the interior of the plot, such as depicted in Fig. 4,

**Table 2** Thermal radiation uniformity {as indicated by the range [(maximum–minimum)/mean] and the coefficient of variation (standard deviation/mean) expressed as a percentages across the defined plot area} across a field plot; geometric and overall efficiencies at wind speeds of 0.0 and 4.0 ms<sup>-1</sup>; annual electrical energy requirements and costs for unlimited heater capacities and for specified heater arrays; and solar shading (nadir view) of various arrays of infrared heaters deployed over field plots

Item	Single heater <sup>a</sup>	Hexagons			Square	Long-narrow <sup>f</sup>
		1 <sup>b</sup>	7 <sup>c</sup>	19 <sup>d</sup>		
Plot Diameter (m) or edge length (m x m)	0.56	3.0	8.0	20	2 × 2 <sup>n</sup>	7.1 × 7.1 <sup>p</sup>
Plot Area (m <sup>2</sup> )	0.25	7.1	50.3	314	4	50.4
No. of Nodes	1	6	24	54	4	–
Fraction on Periphery (%)	100	100	50	33	100	94
Uniformity						
Range (%)	14.1	30.3	36.1	27.3	21.9	31.8
Coefficient of Variation (%)	4.3	7.5	5.4	3.6	4.7	4.6
Efficiency						
Geometric (%)	7.2	37.2	58.0	65.5	26.5	47.4
Overall at 0.0 ms <sup>-1</sup> wind	6.1	31.4	48.8	57.1	22.4	42.2
Overall at 4.0 ms <sup>-1</sup> wind	3.6	25.7	40.6	49.0	18.3	34.5
Infrared heater array power characteristics						
No. of heaters per plot	1 <sup>a</sup>	24 <sup>b</sup>	24 <sup>c</sup>	108 <sup>d</sup>	12 <sup>n</sup>	17 <sup>p</sup>
Power of individual heaters (W)	250	1000	2560	3120	1000	5200
Total power per array (kW per plot)	0.25	24	61.4	337	12	88.4
Unit power (W m <sup>-2</sup> )	1020	3400	1220	1073	3000	1750
Percentage of time 4°C warming can be met under Bondeville, Illinois, USA 2009 weather conditions (%)						
During daytime growing season <sup>e</sup>	0.0	98	85	91	91	97
During nighttime growing season <sup>e</sup>	0.0	100	100	100	100	100
Overall 24-h day, summer and winter	1.7	98	93	96	96	98
Annual electrical energy requirement for 4°C warming under Bondeville, Illinois, USA 2009 weather conditions (MWh per plot)						
For unlimited heater array capacity	14.8	67.8	247	1263	43.8	290
For specified heater array capacity	2.2	66.8	239	1240	43.0	280
Extrapolated from prior 3-m-dimeter <sup>h</sup>	2.0	55.3	393	2460	31.3	394
Growing season <sup>e</sup> electrical energy requirement for 4°C warming under Bondeville 2009 weather conditions (MWh per plot)						
For unlimited heater array capacity	6.3	28.4	111	573	19.5	131
For specified heater array capacity	0.9	28.3	108	565	19.2	126
Annual unit electrical energy requirement (MWh m <sup>-2</sup> )						
For unlimited heater array capacity	60.1	9.6	4.9	4.0	11.0	5.8
For specified heater array capacity	8.9	9.5	4.8	3.9	10.7	5.5
Annual power cost at US\$0.1/kWh (1,000 s of US\$ per plot)						
For unlimited heater array capacity	1.50	6.81	11.1	126	4.40	29.0

**Table 2** (continued)

Item	Single heater <sup>a</sup>	Hexagons			Square	Long-narrow <sup>f</sup>
		1 <sup>b</sup>	7 <sup>c</sup>	19 <sup>d</sup>		
For specified heater array capacity	0.22	6.71	10.8	124	4.28	27.9
Annual unit power cost at US\$0.1 per kWh (\$ m <sup>-2</sup> )				2280		24.0
For unlimited heater array capacity	6010	959	490	402	1100	603
For specified heater array capacity	890	945	476	395	1070	599
Solar Shading (sun directly overhead; %)	25 <sup>i</sup>	4 <sup>j</sup>	6 <sup>k</sup>	6 <sup>l</sup>	4 <sup>o</sup>	3 <sup>r</sup>

The energy and cost estimates were calculated for Bondeville, Illinois, USA using weather from 2009 (e.g., VanLoocke et al. 2010) for 4°C of warming assuming that the vegetation had characteristics similar to 0.5-m-tall alfalfa, and that the vegetation was actively transpiring during growing season (May–September) daytimes whenever the temperature was above freezing and dormant otherwise

<sup>a</sup> Single Mor-ESES 250-W heater at 1.0 m height

<sup>b</sup> Single Hexagon with 24 1,000-W Mor-FTE heaters

<sup>c</sup> Seven-hexagon, 24-node array with 24 2,560-W [0.41 × 0.41 m (16 × 16 in.)] Watlow Raymax 1010 heaters, 1 per node

<sup>d</sup> 19-hexagon, 54-node array with 108 3,120-W [0.31 × 0.66 m (12 × 26 in.)] Watlow Raymax 1010 heaters, 2 per node

<sup>e</sup> 199-hexagon, 450 node array with 900 8,000-W [0.51 × 1.02 m (20 × 40 in.)] Watlow Raymax 1010 heaters, 2 per node

<sup>f</sup> 20 × 2 m long-narrow array with 80 1,000-W Mor-FTE heaters at equal distances along the long edges

<sup>g</sup> May through September

<sup>h</sup> From Kimball et al. (2008; in preparation) for Maricopa, AZ, USA; Cheyenne, WY, USA; and Haibei, Qinghai, China average usage of about 80 kWh/day per plot for 1.5°C of daytime warming on wheat, northern mixed-grass prairie, and grazing land, respectively assuming: (1) that the efficiency is that of the curve fitted to data from the single hexagon arrays (Kimball et al. 2008; Kimball and Conley 2009), (2) that the power usage will be about 80 kWh/day per plot × (4.0/1.5) for 4°C of warming × (area of other plot/7.1 m<sup>2</sup> area of 3-m plot), (3) that this power use applies to actively growing vegetation and half as much is needed when the vegetation is dormant, and (4) that the vegetation is active for 5 months and dormant for 7 months/year

<sup>i</sup> With 0.254-m-diameter reflector, but because of sun angles, only shades about one half of the time

<sup>j</sup> For 24 Mor-FTE heaters (25.4 × 9.9 cm) and because all are around the periphery, assume only shade by one half

<sup>k</sup> For 24 Watlow heaters (0.41 × 0.41 m) assuming the 12 around the periphery shade only one half as much

<sup>l</sup> For 108 Watlow heaters (0.31 × 0.66 m) assuming the 36 around the periphery shade only one half as much

<sup>m</sup> For 900 Watlow heaters (0.51 × 1.02 m) assuming the 108 around the periphery shade only one half as much

<sup>n</sup> 2-m on-a-side square with 12 1,000-W Mor-FTE heaters, 3 at each corner

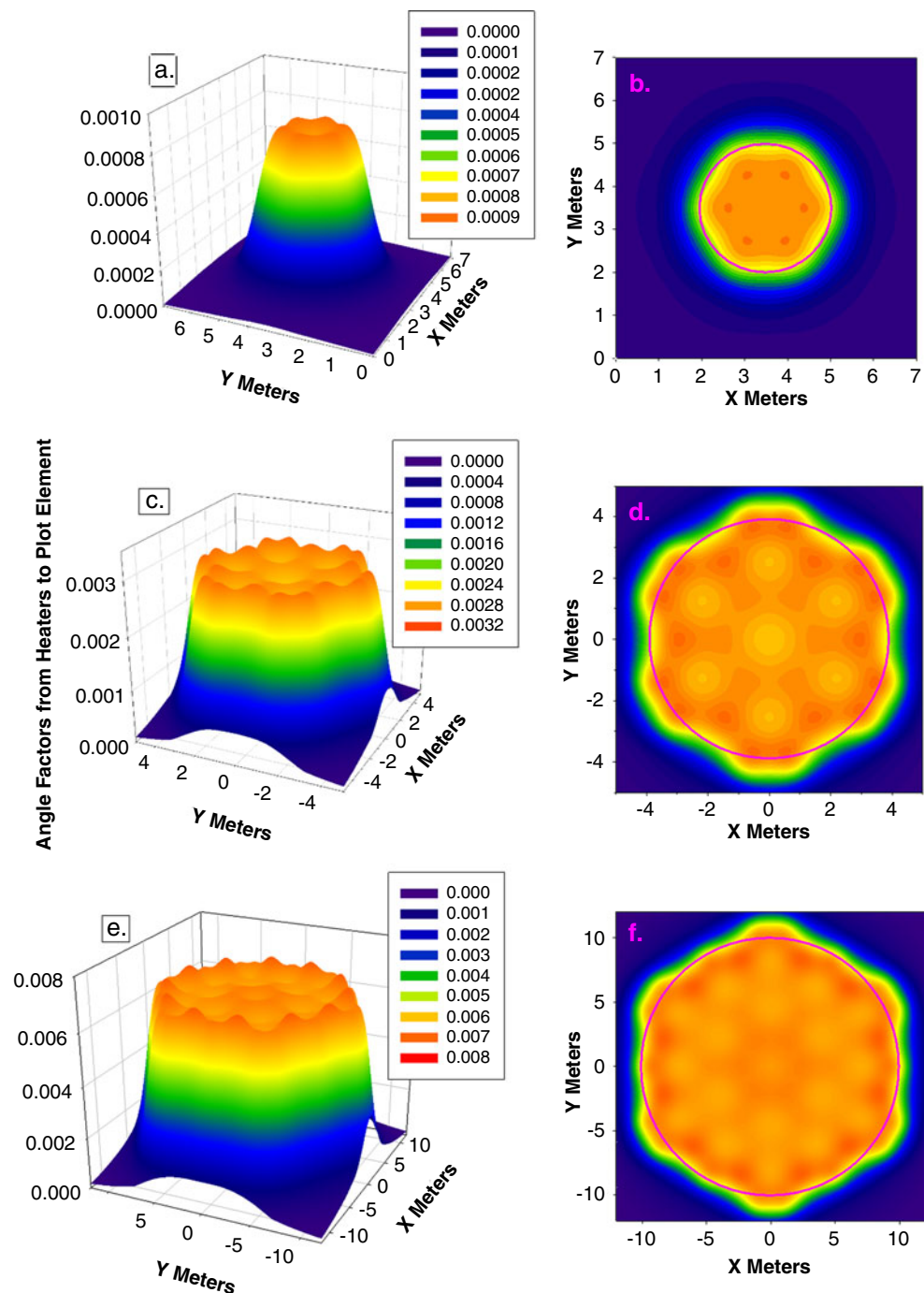
<sup>o</sup> For 12 Mor-FTE heaters (25.4 × 9.9 cm) and because all are around the periphery, assume only shade by one half

<sup>p</sup> 7.1-m on-a-side square with 17 5,200-W [0.51 × 0.66 m (20 × 26 in.)] Watlow Raymax 1010 heaters, 16 at equal distance around the periphery and one in the middle

<sup>q</sup> For 17 Watlow heaters (0.51 × 0.66 m) assuming the 16 around the periphery shade only one half as much

<sup>r</sup> For 80 Mor-FTE heaters (25.4 × 9.9 cm) and because all are around the periphery, assume only shade by one half

**Fig. 3** **a** Color-coded, 3D depiction of the theoretical pattern of angle factors for the down-welling thermal radiation from a hexagonal array of infrared heaters (like Mor FTE, Table 1) deployed at a height of 1.2 m above the vegetation canopy in a 3-m-diameter field plot, such as used by Kimball et al. (2008, in preparation) and Wall et al. (2011). All heaters are tilted at 45° toward the center of the plot. **b** Color-coded contour plot of the pattern from the heater array in (a), where the pink ring denotes the edge of a 3-m-diameter plot. **c** Color-coded, 3D depiction of the theoretical pattern of angle factors for the down-welling thermal radiation from a seven-hexagon array of infrared heaters, such as depicted in Fig. 4. **d** Color-coded contour plot of the pattern from the heater array in (c), where the pink ring denotes the edge of a 8-m-diameter plot. **e** Color-coded, 3D depiction of the theoretical pattern of angle factors for the down-welling thermal radiation from a 19-hexagon array of infrared heaters as depicted in Fig. 4. **f** Color-coded contour plot of the pattern from the heater array in (e), where the pink ring denotes the edge of a 20-m-diameter plot



which has a central hexagon surrounded by additional rings of hexagons. The heaters would be deployed at the nodes where lines in the diagram meet. For 8-m-diameter plots (50.3 m<sup>2</sup>), a seven-hexagon array would be used with a central hexagon and one ring of six additional hexagons. Very good uniformity of the down-welling thermal radiation can theoretically be achieved by using such an array (Fig. 3c, d) with a range of 36.6% and a CV of 5.4% in the angle factors (Table 2).

### 2.5 Nineteen-hexagon array with 54 nodes (20-m scale)

Scaling larger from 8 to 20 m (314 m<sup>2</sup>), it becomes advantageous to add an additional ring of hexagons for a total of 19 hexagons with 54 nodes, as depicted in Fig. 4. At this larger scale, two thirds of the heaters (36 of 54) are interior to the edge of the plot and can be pointed nadir which minimizes loss of radiation outside the plot yet achieves excellent uniformity of the warming treatment

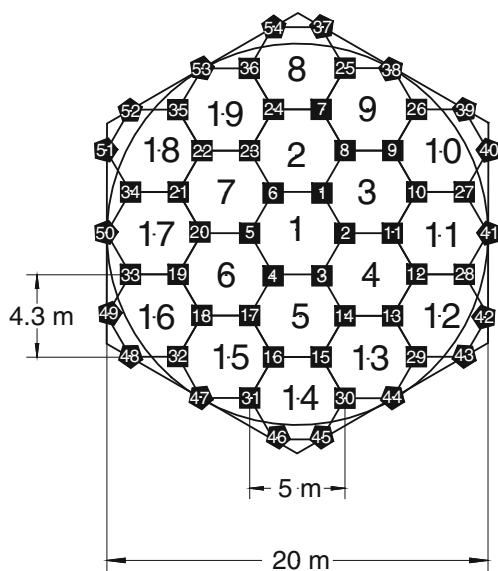


**Fig. 4** Schematic diagram depicting the deployment of infrared heaters over hexagonal plots at 3-, 8-, and 20-m scales. Infrared heaters would be deployed at each of the nodes where lines connect. For the 3-m scale: only the center hexagon #1 would be used as introduced by Kimball et al. (2008). The heaters would be deployed at a height of 1.2 m above the canopy, tilted at 45° from horizontal, and pointed toward the center of the plot. For the 8-m scale: Hexagons #1 through #7 would be used, and the width of an individual hexagon would be 3.2 m. The heaters at each of the 12 outer nodes (7, 9, 10, 12, 13, 15, 16, 18, 19, 21, 22, and 24) would be deployed at 1.28 m, tilted 45° from vertical, and pointed toward the centers of the smaller internal hexagons. The heaters at a mid position between center and outside (nodes 8, 11, 14, 17, 20, and 23) would be deployed at 1.6 m and pointed nadir. The heaters at the central nodes (1–6) would be deployed at 1.92 m and pointed nadir. For the 20-m scale: all 19 of the hexagons in the figure would be used with the width of an individual hexagon being 5 m. The heaters at each of the outer nodes (37–54) would be deployed at a height of 2.25 m above the canopy, tilted at 45° from vertical, and pointed toward the center of the smaller hexagons. The heaters just inside the edge of the plot (nodes 25–36) would be deployed at a height of 2.6 m and pointed nadir. All the rest of the heaters at internal nodes (1–24) would be deployed at 3.5 m and pointed nadir

across the plot (Fig. 3c, d) with a range of 27.3% and CV of 3.6% in the angle factors (Table 2).

**2.6 One hundred ninety-nine hexagon array with 450 nodes (100-m scale)**

In order to study the effects of warming on trees or a structurally variable ecosystem, it is desirable to increase the overall diameter of an infrared heater array to 100 m (7,854 m<sup>2</sup>) or larger. However, the practical upper size limit for individual hexagonal arrays is about 5 m (Fig. 4), or if we anticipate sufficient increases in efficiency, perhaps 8 m. Therefore, we conceived the 199-hexagon honeycomb array shown in Fig. 5a as a possible

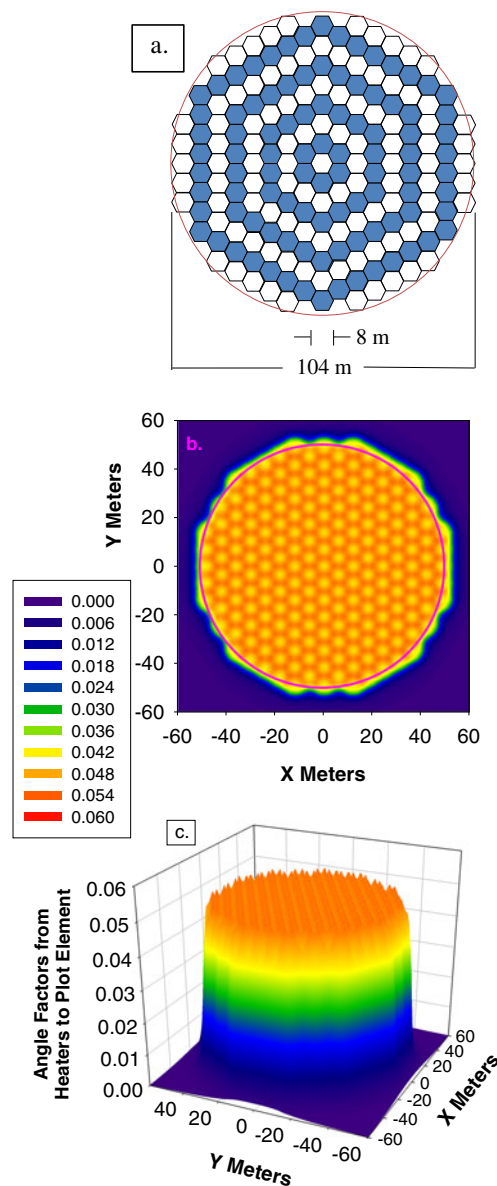


**Fig. 5** a Schematic diagram for the deployment of infrared heaters over a 100-m-diameter plot via the use of 199 internal 8-m-diameter hexagons. Infrared heaters would be deployed at each of the 450 nodes where lines connect. The heaters at each of the 54 outer nodes (where two lines connect) would be tilted at 45° from vertical and pointed toward the center of the particular 8-m hexagon, whereas the heaters at the internal nodes (where 3 lines connect) point nadir. b Color-coded contour plot of the pattern from the heater array in a, where the pink ring denotes the edge of a 100-m-diameter plot. c Color-coded, 3D depiction of the theoretical pattern of angle factors for the down-welling thermal radiation from a 199-hexagon array of infrared heaters as depicted in (a)

configuration to warm 100-m-diameter plots. As can be seen in Fig. 5b and c, the uniformity of the thermal radiation coming from such an array would be excellent, with range of 26.2% and a CV of 5.5% in the angle factors (Table 2).

### 2.7 Square array (2-m scale)

For many experimenters, especially agriculturalists working with row crops, constraints on land availability or plant geometry make it difficult to use circular or hexagonal plots, so square or rectangular plots are often preferred. The first step up from a single heater would be a 2-m-on-a-side ( $4 \text{ m}^2$ ) square configuration, such as shown in Fig. 6a and b. For this case, good uniformity of the treatment can be achieved if the heaters are deployed at a height of 1.1 m above the plant canopy and tilted at  $50^\circ$  from nadir (i.e.,  $\tau=50^\circ$ , Fig. 1). The range in thermal radiation across the plot would be 21.9% and the CV would be 4.7%.

### 2.8 Square array (7-m scale)

Increasing from 2 m on-a-side up to 7.1 m ( $50.4 \text{ m}^2$ ), a configuration with good uniformity is shown in Fig. 6c and d. Sixteen heaters are deployed at equal distances apart around the plot edge, tilted at  $45^\circ$ , and pointed toward the plot center (Fig. 6d). The heaters at the corners are at a height of 1.7 m above the canopy and the others are at 2.0 m. An additional heater is deployed at 2.3 m at the plot center and pointed nadir. This configuration has a range in angle factors across the plot of 31.8% and a CV of 4.6% (Table 2).

### 2.9 Long-narrow array ( $2 \times 20$ -m scale)

Experimenters who work with row crops often find it advantageous to work with long rows of vegetation. Such a case is depicted in Fig. 6e and f for a 2 m wide by 20 m long plot, for which we envision heaters deployed along the edges of the plot and tilted toward the long axis. After trying various heights and tilts, it was found that a height above the vegetation of 1.0 m and a tilt of  $45^\circ$  was close to optimum. It produced a range of 55.7% and a CV of 10.2% of the angle factors across the plot, which is worse than any of the hexagonal or square arrays (Table 2).

## 3 Infrared heater array efficiency

As defined in the “Introduction,” there are two aspects that control the efficiency with which electrical power delivered to an infrared heater array results in thermal radiation impinging on a field plot. One is the “radiometric efficiency,” which is the percentage of the electrical power supplied to the heaters that results in thermal radiation emitted by the heaters rather than lost by forced convection to wind or natural convection from buoyant air currents. The second is the “geometric

efficiency,” which is the percentage of the thermal radiation emitted by the heaters that lands within the plot area. The “overall efficiency” is the product of the radiometric and geometric efficiencies.

### 3.1 Radiometric efficiency

Kimball (2005) presented theory to predict the radiometric efficiency of infrared heaters based on convective heat transfer equations from Campbell (1977). The equations are based on prior work using flat plates in laminar flow, so real heaters in the more turbulent outdoors may have higher convective heat transfer coefficients and consequently somewhat lower efficiencies than the theoretical values. Nevertheless, the theory is useful for predicting approximate performance, and we calculated the radiometric efficiency of the heaters listed in Table 1 as a function of wind speed (Fig. 7). The coefficient for natural convection at low wind speed varies with the tilt of a heater. It is maximum for a plate or heater tilted to face sideways and somewhat less for a heater pointed upward (e.g., Monteith 1973). For a heater pointed downward, the coefficient is about one half that of a heater facing upward (e.g., Campbell 1977). For the calculations presented herein, we assumed that for heaters tilted at  $45^\circ$ , the coefficient for natural convection was the same as that of a heated plate facing upward, whereas for heaters pointed down, the coefficient was one half that of an upward facing plate.

Huge differences in theoretical radiometric efficiency exist among various designs of infrared heaters (Fig. 7) due to their differing characteristic dimensions, which govern how their performance is affected by wind speed. Because of the small characteristic dimension of the rod-shaped Kalglo heater and its low emissivity, its theoretical radiometric efficiency is the lowest among the several heaters examined. On the other hand, it has a large reflector housing, which may shield the heating element somewhat, so its radiometric efficiency is probably somewhat higher than the theoretical curve. Looking at the theoretical curves for the other heaters in Fig. 7, it is apparent that increasing the heater’s emissivity and increasing its characteristic dimension greatly improve radiometric efficiency. A comparatively large  $1.02 \times 1.02$ -m heater from Watlow (actually two adjacent  $1.02 \times 0.51$ -m heaters) oriented nadir would have radiometric efficiencies ranging from about 93% to 66% for wind speeds from 0 to  $14 \text{ ms}^{-1}$ .

Besides the characteristic dimension, power density also varies among the heater models (Table 1), and it also affects radiometric efficiency because the operating temperature of the emitting surface affects the proportion of energy emitted as radiation versus convective loss. The Mor-FTE heater has a power density of about  $68 \text{ kW m}^{-2}$  compared to  $15.4 \text{ kW m}^{-2}$  for the Watlow Raymax 1010 (Table 1); yet, the smaller

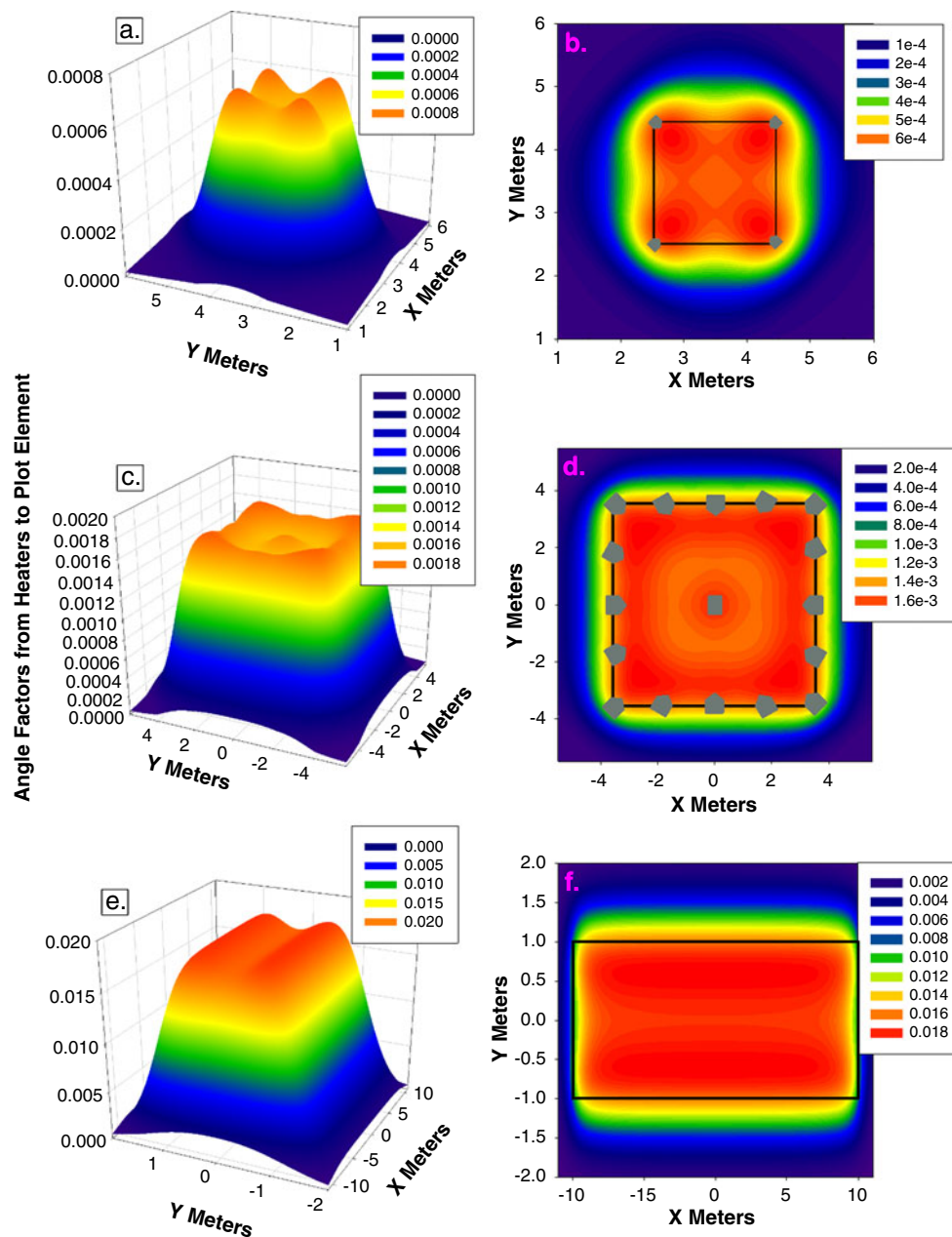


**Fig. 6** **a** Color-coded, 3D depiction of the theoretical pattern of angle factors for the down-welling thermal radiation from a square array of infrared heaters (like Mor FTE, Table 1) deployed at a height of 1.1 m above the vegetation canopy at the corners of a 2-m $\times$ 2-m square field plot. All heaters are tilted at 50° from nadir (i.e.,  $\tau=50^\circ$ , Fig. 1) toward the center of the plot. **b** Color-coded contour plot of the pattern from the heater array in **a**, where the *black square* denotes the edge of a 2-m $\times$ 2-m square plot, and the *gray spots* indicate the heaters and the direction they point. **c** Color-coded, 3D depiction of the theoretical pattern of angle factors for the down-welling thermal radiation from a 7.1-m $\times$ 7.1-m square array of infrared heaters. **d** Color-coded contour plot of the pattern from the heater array in **(c)**, where the *black square* denotes the edge of a 7.1-m $\times$ 7.1-m square plot, and the *gray spots* indicate the heaters and the direction they point. The center heater is deployed at

2.3 m above the vegetative canopy and pointed nadir. The heaters at the corners are deployed at 1.7 m, tilted by 45°, and pointed toward the center (45° from edge of the plot). The other heaters on the periphery are deployed at 2.0 m, tilted at 45°, and point toward the center of the plot (60° from the edge of the plot for those next to the corners and 90° for those at the midway point of an edge). **e** Color-coded, 3D depiction of the theoretical pattern of angle factors for the down-welling thermal radiation from a long-narrow (2 $\times$ 20 m) array of infrared heaters. Note the large difference in scale for the *X* and *Y* directions. **f** Color-coded contour plot of the pattern from the heater array in **(e)**, where the *square rectangle* denotes the edge of the long-narrow plot. Infrared heaters would be deployed above the long edges of the plot at 1.0 m above the vegetative canopy and tilted at 45° toward the long-axis center

Mor-FTE (60 mm) has higher radiometric efficiencies than larger Watlows (0.15 and 0.30 m) (Fig. 7). However, the

largest Watlows (0.41 m and larger; Fig. 7) should have greater radiometric efficiencies than the Mor-FTE.

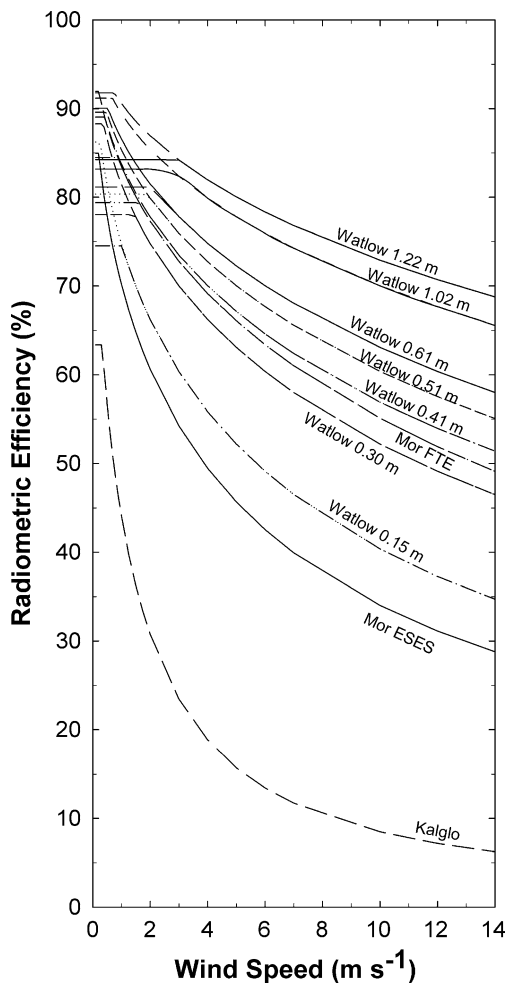


**Fig. 7** Theoretical radiometric efficiencies of several infrared heaters calculated using the theory derived by Kimball (2005). The characteristics of the heaters are listed in Table 1. Going from high to lower wind speeds, the curves for the Watlow heaters bifurcate due to the two different natural convection coefficients for two different tilts. The *lower branches* are for heaters tilted at  $45^\circ$  and *upper branches* for heaters pointed down. The Mor-FTE curve is for heaters tilted at  $45^\circ$ . The theory is based on flat plate equations from Campbell (1977) for air at  $20^\circ\text{C}$  and 100 kPa pressure. For heaters tilted at  $45^\circ$ , the coefficient for natural convection at low wind speed was assumed to be the same as that of a heated plate facing upward, whereas for heaters pointed down, the coefficient was one half that of an upward facing plate

### 3.2 Geometric efficiency

Geometric efficiency accounts for losses due to thermal radiant energy falling outside the plot area. If an infrared heater is very close to the surface being warmed, then the geometric efficiency would approach 100%, whereas if a heater is raised to ever higher elevations above a plot, more and more radiation will fall outside the plot area, thereby lowering geometric efficiency. Furthermore, when the heaters are tilted away from nadir, more radiation can escape to the sky, and potentially other areas outside the

plot in the direction the heater is pointed. Manufacturers of many models of infrared heaters add reflectors of various designs to try to improve their heater's geometric efficiency by redirecting some of the thermal radiation that would otherwise be lost. The angle factor calculations for planar black bodies in the previous section on thermal radiation distribution uniformity do not include reflectors, so opportunities may exist for using reflectors to improve their geometric efficiency. However, improvements in geometric efficiency with reflectors will likely come at the cost of greater solar shading.

The angle factor methodology described in the previous section on radiation uniformity was used to calculate the theoretical geometric efficiency of several infrared heater arrays (Table 2). Of course, the choice of exactly where plot boundaries lie and how large the plots are affects geometric efficiency. For the case of a single Mor ESES heater at a height of 1 m above the vegetation canopy, Bijoor et al. (2008) stated their usable plot diameter was 0.56 m (Fig. 2b). This choice results in excellent radiation uniformity ( $\text{CV}=4.3\%$ ), but the geometric efficiency is only 7.2% (Table 2). In contrast, the equivalent diameter for Hovenden et al. (2006) was 1.2 m (Fig. 2b), which results in poor radiation uniformity ( $\text{CV}=193\%$ ), but geometric efficiency improves to 9.6%.

Moving on to multiple heater arrays whose thermal radiation distribution has the shape of the frustum of a cone (Fig. 3), the plot diameter boundary is more easily defined. For a single hexagonal array such as used by Kimball et al. (2008) with a plot diameter of 3 m and heaters deployed at a height above the vegetation of 1.2 m (Fig. 3a, b), the theoretical geometric efficiency is 37.2% (Table 2), much higher than that for a single heater. The seven-hexagon 8-m-diameter array shown in Figs. 3c, d and 4 has a central hexagon with downward pointing heaters at a height 4.8 m and another six nodes between the center hexagon and periphery with downward pointing heaters at 4.0 m, but only 50% of its heaters are on the periphery ( $45^\circ$  tilt at height of 3.2 m). As a result, its geometric efficiency improves to 58.0% (Table 2). Increasing plot diameter still further to 20 m, adding another ring of hexagons becomes appropriate (Figs. 3e, f, 4), so there are a total of 19 hexagons with 54 nodes and a resultant increase in geometric efficiency to 65.5% (Table 2). Scaling further to 100 m with the 199-hexagon array shown in Fig. 5, which has 450 nodes all a height 4.0 m above the canopy, the proportion of the heaters tilted at  $45^\circ$  on the periphery becomes smaller yet (12%), and geometric efficiency increases to an impressive 83.6% (Table 2).

As mentioned previously, many scientists, especially those working with row crops, prefer rectangular plots, for which arrays of infrared heaters with respectably uniform distribution of the radiation can be designed (Fig. 6).

However, the geometric efficiencies tend to be lower (Table 2). For example, the  $7.1 \times 7.1$ -m square array (Figs. 6c, d) has the same area ( $50 \text{ m}^2$ ) as an 8-m-diameter hexagonal array (Figs. 3c, d) but the geometric efficiency for the square is 47.4% compared to 58.0% for the hexagon (Table 2).

### 3.3 Overall efficiency

As defined previously, overall efficiency is the fraction of the electrical power supplied to an infrared heater array that results in thermal radiation impinging within a field plot, and it is the product of the radiometric and geometric efficiencies. Because the area of uniform thermal radiation is so small beneath a single Mor-ESES heater (Fig. 2, 0.56-m diameter), its geometric efficiency is low (7.2%; Table 2), and the resultant overall efficiency is also low (6 to 2%; Fig. 8). In contrast, for a Kalglo heater, the radiometric efficiency is low (Fig. 7), but the reflector improves geometric efficiency compared to a planar black-body radiator, so the overall efficiency is somewhat better than that of a Mor-ESES heater (Fig. 8). Mor-FTE heaters have emissivities close to 1.0, and their power densities are comparatively higher (Table 1), so their radiometric efficiency is higher than that of individual Kalglo and Mor-ESES heaters (Fig. 7). Coupled with a much higher geometric efficiency for a hexagonal array of such heaters (Table 2), the resultant overall efficiency of a hexagonal array ranges from about 35% at zero wind to 18% at wind speeds of  $14 \text{ ms}^{-1}$  (Fig. 8). With the exception of very low wind speeds, this efficiency is much higher than a single Mor-ESES heater or a single Kalglo heater (Fig. 8). The larger physical size of Watlow heaters (Table 1) imparts a higher radiometric efficiency (Fig. 7), which coupled with the higher geometric efficiencies of the larger 7-, 19-, and 199-hexagonal arrays (Table 2), results in very much higher overall efficiencies for multiple hexagon honeycomb arrays (Fig. 8). Indeed, a seven-hexagon, 8-m-diameter array with 0.41-m heaters would have efficiencies ranging from about 49% at zero wind to 30% at  $14 \text{ ms}^{-1}$ ; the efficiencies of 199-hexagon, 100 m array with 1.02-m heaters would range from about 75% at zero wind to 55% at  $14 \text{ ms}^{-1}$ . As expected, the overall efficiency curve for a  $2\text{-m} \times 2\text{-m}$  square is higher than that for a single heater but lower than a 3-m-diameter hexagon (Fig. 8). The curves for the  $7.1 \times 7.1$ -m square with 0.51-m Watlow heaters and the long-narrow  $2 \times 20$  m rectangle with Mor-FTE heaters are similar and intermediate between those for single- and seven-hexagon arrays. Equations that describe the overall efficiency versus wind speed curves for eight of the array-heater combinations shown in Fig. 8 are presented in Table 3.

Besides the theoretical overall efficiencies shown in Fig. 8, measured efficiencies for a Kalglo heater from Kimball (2005) and for hexagonal arrays of Mor-FTE

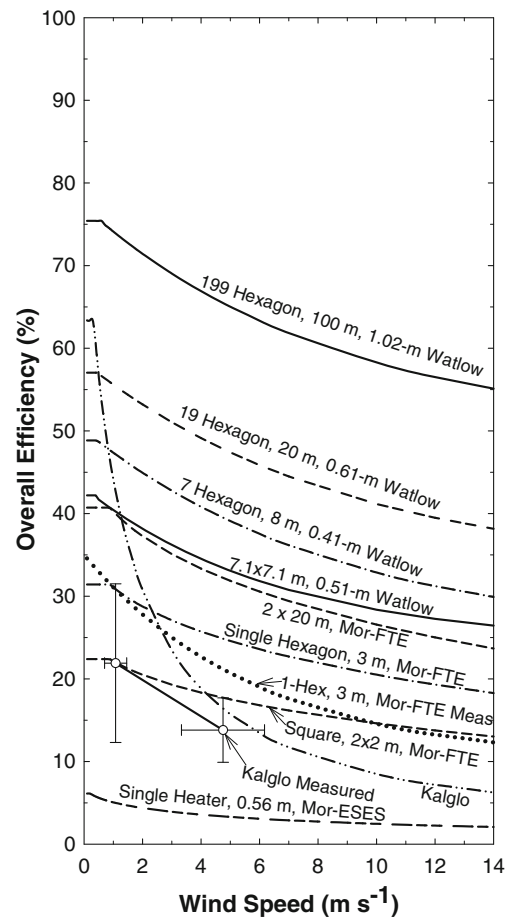


**Fig. 8** Overall efficiencies (radiometric efficiency (Fig. 7) times geometric efficiency (Table 2) for several arrays of infrared heaters including: (1) 199-hexagon, 450-node, 100-m-diameter array (Fig. 5) with banks of two Watlow heaters ( $0.51 \times 1.02 \text{ m}$ ; Table 1) at each node; (2) 19-hexagon, 54-node, 20-m-diameter array (Figs. 3e, f, 4) with banks of two Watlow heaters ( $0.31 \text{ m} \times 0.66 \text{ m}$ ; Table 1) at each node; (3) 7-hexagon, 24-node, 8-m-diameter array (Figs. 3c, d, 4) with a Watlow heater ( $0.41 \text{ m} \times 0.41 \text{ m}$ ; Table 1) at each node, (4) single hexagon, 3-m-diameter array (Figs. 3a, b) with theoretical efficiency of Mor-FTE heaters (Table 1); (5) single hexagon, 3-m-diameter array (Figs. 3a, b) with measured efficiency (Kimball et al. 2008) of Mor-FTE heaters (Table 1); (6) single Kalglo heater assuming 100% geometric efficiency and theoretical radiometric efficiency; (7) single Kalglo heater with measured efficiency (Kimball 2005); (8) single Mor-ESES heater at 1 m over 0.56-m-diameter plot; (9) square  $7.1 \times 7.1 \text{ m}$  array (Figs. 6c, d) with  $0.51 \times 0.66 \text{ m}$  Watlow heaters; (10) long-narrow  $2 \times 20 \text{ m}$  array (Figs. 6e, f) with Mor-FTE heaters; and (11) square  $2 \times 2 \text{ m}$  array (Fig. 6a, b) with Mor-FTE heaters)

heaters from Kimball et al. (2008) and Kimball and Conley (2009) are plotted. The measured values for the Kalglo heater are much lower at low wind speeds than the theoretical values but come into agreement at about  $5 \text{ ms}^{-1}$ . The theoretical and measured values for the single hexagon agree fairly well at low wind speeds, but the measured values are somewhat lower at high winds. Nevertheless, there is sufficient agreement between the theoretical curves and the measured curves to give

**Table 3** Equations to describe the overall efficiencies,  $\eta$  (%), of various infrared heater arrays in Fig. 8 as a function of wind speed,  $u$  ( $\text{m s}^{-1}$ )

Array	Equation
Single heater, 0.56-m plot, Mor-ESES	$\eta = 2.114 + 3.916 \times \exp(-0.2586 \times u)$
Single hexagon, 3.0-m plot, Mor-FTE	$\eta = 10 + 25 \times \exp(-0.17 \times u)$
7-hexagon, 8.0-m plot, 0.41-m Watlow	If $u > 0.4472$ , $\eta = 24.77 + 25.33 \times \exp(-0.1141 \times u)$ ; otherwise, $\eta = 48.84$
19-hexagon, 20.0-m plot, 0.61-m Watlow	if $u > 0.4473$ , $\eta = 32.78 + 25.51 \times \exp(-0.1114 \times u)$ ; otherwise, $\eta = 57.05$
199-hexagon, 100-m plot, 1.02-m Watlow	if $u > 0.5574$ , $\eta = 49.83 + 27.31 \times \exp(-0.1144 \times u)$ ; otherwise, $\eta = 75.41$
Square, 2 m $\times$ 2 m, Mor-FTE	if $u > 0.7383$ , $\eta = 11.43 + 12.14 \times \exp(-0.1385 \times u)$ ; otherwise, $\eta = 22.39$
Square, 7.1 m $\times$ 7.1 m, 0.51-m Watlow	if $u > 0.3144$ , $\eta = 24.12 + 18.95 \times \exp(-0.1495 \times u)$ ; otherwise, $\eta = 42.20$
Long-narrow, 2 $\times$ 20 m, Mor-FTE	if $u > 0.7212$ , $\eta = 20.73 + 22.09 \times \exp(-0.1385 \times u)$ ; otherwise, $\eta = 40.72$

The equation for the single hexagon is from the measured data of Kimball et al. (2008) and Kimball and Conley (2009), whereas the other equations are based solely on the theoretical calculations presented herein. For the 7-, 19- and 199-hexagon arrays and the 7.1 $\times$ 7.1 m square (Figs. 3–6) the values for radiometric efficiency (Fig. 7) were weighted for the number of inside heaters pointed nadir and the number of peripheral heaters tilted at 45°

confidence that the theory is correct to at least a first-order approximation.

#### 4 Energy requirements and costs

From the overall efficiencies such as presented in the previous section (Fig. 8; Table 3) and computations of the amounts of additional radiation required to raise the temperature of vegetative canopies by given degrees of warming, the amounts of electrical energy required per square meter of ground area for the given degrees of warming can be calculated. Kimball (2005) derived an equation that predicts the amount of additional thermal radiation required to warm a plant canopy as a function of microclimatic and plant parameters for an incremental amount of warming. However, he did not account for buoyancy effects well, so more recently, Kimball et al. (in preparation) derived another procedure that utilizes the well-accepted Monin–Obukhov Similarity Theory (MOST; e.g., Ham (2005)) for calculating aerodynamic resistance. Convergence problems were encountered when iterating for solutions, so a hybrid procedure was adopted whereby the equations of Mahrt and Ek (1984) were used to obtain the initial starting values for the iterative process using MOST. Kimball et al. (in preparation) report that the hybrid procedure eliminated the convergence problems most of the time, and for those hours when convergence was not obtained, they generally could interpolate values from the previous and following hours.

To calculate the annual energy requirements of several sizes of infrared heater arrays (Table 2) for illustrative and experimental planning purposes, we chose weather data from a site in Illinois because it is representative of a large, agriculturally important region of the USA. Hourly weather data (solar radiation, air temperature and relative humidity, and wind speed at 10-m height) for 2009 were obtained from the Department of Atmospheric Sciences, University

of Illinois, specifically the Bondeville site, which is part of the NOAA Surface Radiation Network (SURFRAD; <http://www.srrb.noaa.gov/surfrad/bondvill.html>; e.g., VanLoocke et al. 2010). In 2009, average wind speeds were 5.2 and 4.4  $\text{ms}^{-1}$  during day and nighttime, respectively, which corresponds to about 3.4 and 2.9  $\text{ms}^{-1}$ , respectively, when adjusted to 2-m height for 0.5-m-tall vegetation. Therefore, the windiness at this site is about midway between the windy Cheyenne, WY site (5.7 and 4.2  $\text{ms}^{-1}$  for day and night, respectively) and the calmer Maricopa, AZ site (2.2 and 1.8  $\text{ms}^{-1}$  for day and night, respectively) that were studied by Kimball et al. (2008).

The following assumptions were made: (1) the vegetation canopy architecture and stomatal characteristics were similar to those of 0.5-m-tall alfalfa, for which standardized equations exist for predicting evapotranspiration (ET; minimum daytime canopy resistance of 30  $\text{sm}^{-1}$  and nighttime canopy resistance of 200  $\text{sm}^{-1}$ ; Allen et al. 2005), and (2) the vegetation was actively transpiring and not water-stressed during daytimes when temperatures were above freezing, but it was dormant (canopy resistance= 200  $\text{sm}^{-1}$ ) when temperatures were below freezing. Then, using the hourly weather data, electrical energy requirements were calculated for 4°C of warming for every hour of 2009 using the efficiency equations for the eight infrared heater arrays listed in Table 3. The calculations were done following Kimball et al. (in preparation) using the hybrid Mahrt and Ek/MOST procedure for aerodynamic resistance. Following Monteith (1973), the roughness length was calculated as 0.13 times plant height, and the displacement height was calculated as 0.63 times plant height. For the 0.5-m-tall alfalfa, convergence was obtained for every hour, whereas when runs were made for 1.0-, 2.7-, 6.7-, 7.0, and 33.3-m-tall vegetation, convergence was not obtained for 6, 44, 84, 88, and 216 h out of the 8,760 h of the year. For these non-convergent times, interpolations were made using results from the previous and following hours when

convergence had been obtained. The results were sorted into six groups: growing season daytime, nighttime, and 24-h days; and whole year daytime, nighttime, and 24-h days. Various sums are listed in Table 2, and cumulative fraction histograms for the summer days are plotted in Fig. 9.

As sizes of plots and heaters increase, the corresponding increases in overall efficiency (Fig. 8; Table 3) result in progressively lower heater power requirements per unit area (Fig. 9). The power requirements per unit area for the 100-m plot are about one sixth of those for the 3-m plot. The power requirements for the single heater, 0.56-m plot are an order of magnitude larger than those of the other arrays, which necessitated the break and change of scale in the  $x$ -axis. Comparing the curves for 199-hexagon, 100-m plots for alfalfa and trees, increasing plant height from 0.5 to 7.0 m more than doubles the power requirements. Although not shown, the curves for growing season nighttime are about half as large as those for growing season daytime, consistent with lower ET due to stomatal closure and with calmer winds at night. The curves for all year, 24-h days are intermediate between the growing season nighttime and daytime values.

Cumulative fraction curves (Fig. 9) are most useful for estimating the percentages of time that various heater arrays can meet the desired  $4^{\circ}\text{C}$  warming target. The thin vertical dashed line at  $2,000\text{ W m}^{-2}$  in Fig. 9 corresponds to the heater capacity for 80 1,000-W Mor-FTE infrared heaters

deployed along the edges of the long sides of a  $2\times 20$ -m plot with  $4^{\circ}\text{C}$  of warming. The horizontal dashed line indicates where the 2000 line crosses the daytime cumulative fraction curves for the  $2\times 20$ -m plot. Following the horizontal line to the  $y$ -axis, the cumulative fraction of daylight hours that this 80-heater array can meet the  $4^{\circ}\text{C}$  target is 0.98. In other words, 80 of the 1,000-Watt Mor-FTE heaters should be able to meet the heating requirement for 98% of the growing season daylight hours for a  $2\times 20$ -m plot if all the assumptions are met.

Using the curves in Fig. 8 for growing season daytimes and similar curves (not presented) for growing season nights and whole-year, 24-h days, the percentages of time that the eight types of arrays can meet the  $4^{\circ}\text{C}$  heating requirement were estimated (Table 2). The single Mor-ESES heater would be far too weak and not able to achieve  $4^{\circ}\text{C}$  of warming during any of the growing season hours. In contrast, the other arrays should be able to achieve the warming from 85% to 98% of the daylight hours. On growing season nights, these arrays should be able to provide the  $4^{\circ}\text{C}$  of warming all the time (within rounding error). Considering the overall whole-year, 24-h day cases, these seven arrays should achieve the warming from 93% to 99% of the time.

The hourly data were summed for all hours in 2009 to obtain annual electrical energy requirements for the eight types of arrays (Table 2). The requirements were 14.8, 67.8,

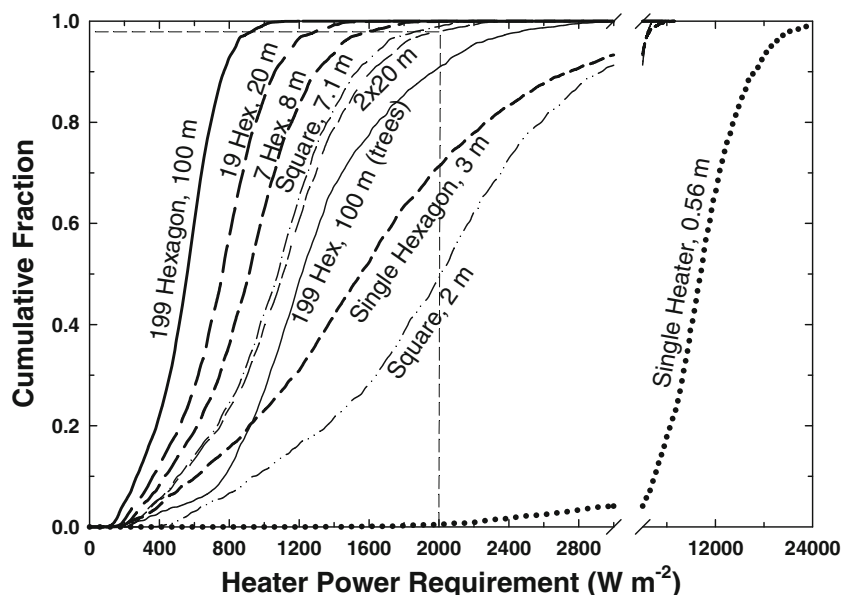


**Fig. 9** Cumulative fractions of hourly electrical energy requirements for eight types of infrared heater arrays (Table 2) over open-field plots for  $4^{\circ}\text{C}$  of warming using 2009 weather data from Bondeville, IL, USA growing season (May–September) daytime conditions. The overall efficiency equations corresponding to each array from Table 3 were used. The vegetation properties were those of 0.5-m-tall alfalfa (Allen et al. 2005) assuming no water stress (i.e., maximum evapotranspiration) except for one curve for which the vegetation had the same minimum canopy conductance as alfalfa ( $30\text{ sm}^{-1}$ ) but

the roughness length and displacement height of 7-m-tall trees. To illustrate the utility of the curves, for example, 80 1,000-W Mor-FTE heaters deployed along the edges of a long-narrow plot ( $2\times 20$  m) amounts to  $2,000\text{ W m}^{-2}$  of heater capacity. Locating 2000 on the  $x$ -axis and following the *dashed line* upward to the  $2\times 20$ -m curve and then horizontally to the  $y$ -axis at 0.98 means that the array should meet the daytime heating requirement about 98% of the growing seasontime daylight hours

247, 1,263, and 22,890 MWh per plot for the 0.56-, 3-, 8-, 20-, and 100-m-diameter plots, respectively. However, some of the time, especially under windy conditions, the heaters would be fully on and yet unable to meet the heating requirements, so the actual power consumed would be only that of the heater capacity. Therefore, the energy consumptions were calculated for the specified heater capacities, and they amounted to 2.2, 66.8, 239, 1,240, and 22,770 MWh per plot, respectively. For the  $2 \times 2$ -,  $7.1 \times 7.1$ -, and  $2 \times 20$ -m rectangular plots, the respective annual requirements were 43.8, 290, and 241 MWh per plot.

Based on the prior observations of Kimball et al. (2008, in preparation) that about 80 kWh/day per plot are required with 3-m plots, we assumed the same efficiency curve (which was determined to be the same for both 3- and 5-m plots (Kimball and Conley 2009)) applies and extrapolated from 1.5°C to 4.0°C of warming and from 7.1 m<sup>2</sup> to the areas of the other arrays (Table 2). In making this extrapolation, we also assumed that the vegetation was dormant from October through April; therefore, energy requirements were reduced by one half during this time. This extrapolation suggests a slightly lower annual energy requirement for the 3-m plot (55.3 versus 67.8 MWh), but for the 100-m plot, the extrapolated energy requirement is 2.7 times the theoretically calculated one (61,400 versus 22,890 MWh per plot) (Table 2).

The large increase in annual energy requirements with increasing plot area masks the effects of efficiency which also increase with plot area and with the characteristic dimension of the larger heaters chosen for the larger arrays. Annual energy requirements per square meter would be 60.1, 9.59, 4.90, 4.02, and 2.92 MWh m<sup>-2</sup> for the 0.56-, 3-, 8-, 20-, and 100-m-diameter plots, respectively, so there would be, in fact, a large economy of scale with larger plot sizes (Table 2). The square and rectangular plots similarly exhibit an economy of scale going from 11.0 to 5.75 MWh m<sup>-2</sup> for the  $2 \times 2$ - to  $7.1 \times 7.1$ -m plots, respectively.

Electrical energy prices vary region by region and even by time of day but currently are often close to US\$0.1/kWh (<http://www.eia.doe.gov/>). Using this price assumption, annual electrical energy requirement values were multiplied by 0.1 to estimate annual power costs (Table 2). For unlimited heater array capacities, the annual power costs would be about US\$1,500, US\$6,810, US\$11,100, US\$126,000, and US\$2,290,000 per plot for the 0.56-, 3-, 8-, 20-, and 100-m-diameter plots, respectively. For the specified heater capacity configurations, the corresponding values are US\$220, US\$6,710, US\$10,800, US\$124,000, and US\$2,280,000 per plot, respectively. Putting the latter values on a unit area basis, the costs would be about US\$890, US\$945, US\$476, US\$395, and US\$290 m<sup>-2</sup>, respectively, again illustrating the economy of scale for larger arrays.

The results presented in Table 2 and Fig. 9 illustrate the effects of increasing the efficiency of infrared heater arrays on electrical power requirements due to increasing the characteristic dimension of the heaters and of increasing the proportion of internal versus peripheral heaters as plot area increases for “standard” 0.5-m tall alfalfa vegetation. However, a major incentive for using larger plots is to be able to warm larger stature vegetation, including trees. We (e.g., Kimball et al. 2008, in preparation; Wall et al. 2011) have found that the T-FACE system with a single hexagon array over a 3-m-diameter plots works well for vegetation at least as tall as 1-m wheat. Therefore, we did additional calculations for the 3-, 8-, 20-, and 100-m-diameter plots but for vegetation whose height was one third the plot diameter (Table 4). Because heater heights are determined with respect to the top of the vegetative canopies (Fig. 1), they were unchanged. However, for the 33.3-m-tall trees in the 100-m plot, we arbitrarily changed the measurement height of the weather data from 10 to 50 m so as to be above the canopy. The same overall efficiency equations were used (Table 3), although the results suggested that larger heaters with slightly larger efficiencies would be appropriate

**Table 4** Annual electrical energy requirements for 4°C of warming for the 3-, 8-, 20-, and 100-m-diameter infrared heater arrays listed in Table 2

Item	Plot diameter (m)			
	3	8	20	100
Number of hexagons	1	7	19	199
Height of vegetation (m)	1.0	2.7	6.7	33.3
Annual electrical energy requirement (MWh per plot)	81.4	422	4150	77600
Ratio compared to 0.5-m-tall alfalfa (Table 2)	1.20	1.71	3.29	3.39
Ratio compared to extrapolations from measured in 3-m plots (Table 2)	1.47	1.07	1.67	1.27
Annual electrical energy requirement (MWh m <sup>-2</sup> )	11.5	8.4	13.2	9.9

The difference from Table 2 is that rather than 0.5-m-tall alfalfa, the vegetation is assumed to have a height that is one third of the plot diameter. Hourly weather data from Bondeville, IL, USA (e.g., VanLoocke et al. 2010) was again used. The day and nighttime canopy resistances were taken as 30 and 200 sm<sup>-1</sup>, respectively, the same as “standard” alfalfa (Allen et al. 2005). It was also assumed that the vegetation was non-stressed and actively transpiring whenever the temperature was above freezing and dormant otherwise

in order to meet the energy requirements greater fractions of the time. The annual electrical energy requirements amounted to 81.4, 422, 4150, and 77600 MWh per plot for the 3-, 8-, 20-, and 100-m-diameter plots, respectively. Compared to 0.5-m tall alfalfa (Table 2), the increased stature of the vegetation increased energy requirements by 1.20, 1.71, 3.29, and 3.39, respectively (Table 4). On a unit area basis, the requirements were 11.5, 8.4, 13.2, and 9.9 MWh m<sup>-2</sup>, respectively. Thus, while the increasing efficiency with increasing plot and heater sizes imparts an economy of scale (Table 2), the decrease in aerodynamic resistance due to the larger stature vegetation that likely would be grown in the larger plots would negate the improvement in efficiency, and extrapolations from measurements in 3-m plots would not be greatly in error (Table 4).

## 5 Solar shading

As addressed in the “Introduction,” it is desirable that infrared heater arrays not shade the vegetation from solar radiation, but such is not generally feasible except at high latitudes (e.g., Nijs et al. 1996). Of course, sun angles are continually changing at any location with season and time of day. However, to get an idea of the amount of shading to be expected, we calculated the projected area of the heaters with the sun directly overhead. We ignored shading from any structure that would be in place to deploy the heaters over the plots on the assumption that the projected area of the structures would be a small fraction of the area of the heaters themselves. A single Mor-ESES heater with 0.254-m-diameter reflector over a 0.56-m-diameter plot would shade the plot by 25% (Table 2). However, this is probably not a fair value for this tiny plot because anytime the sun’s angle is more than 22° from zenith, the heater’s shadow would not fall on the plot. For all the other arrays, however, it would take very large solar zenith angles for there not to be some shading of the plot. Accordingly, we assumed that all heaters internal from the edge would shade the plot fully, whereas only half of those around the periphery would shade at any particular time. Consequently, the solar shading would be about 4%, 6%, 6%, and 6% for the 3-, 8-, 20-, and 100-m-diameter plots, respectively. For the 2 × 2-, 7.1 × 7.1-, and 2 × 20-m plots, the shading would be about 4%, 6%, and 3%, respectively.

## 6 Discussion

One way to assess the feasibility of conducting infrared warming experiments on large plots with tall stature vegetation would be to linearly extrapolate with area and with degrees of warming from the 3-m-diameter plots with

1.5°C warming that are already in use. However, by utilizing methodology derived by Kimball (2005) to account for increasing radiometric efficiency with increasing size of the heaters and utilizing the equations derived herein to additionally account for increasing geometric efficiency with increasing plot size, it appears that the operating costs for energy would be about one third those obtained by such an extrapolation (Table 2). Nevertheless, it is still apparent that such large-plot experiments will be expensive in comparison to most research budgets.

In order to estimate energy requirements and costs, we chose a particular ecosystem. However, plant canopies vary immensely in their architecture, and their stomatal conductance changes drastically from night to day and, at least for temperate climates, from summer to winter. Furthermore, microclimatic variables, among which wind speed is especially important, are continually changing from night to day and from one weather pattern to another. Therefore, the cost of an infrared warming treatment in any experiment will depend greatly on the ecosystem selected for study, the local climate, and the vagaries of weather.

One severe constraint in the designs we presented (Figs. 3–6) is that proportionally large infrared heaters are not commercially available. Therefore, one avenue to explore would be to induce a manufacturer to build larger heaters or possibly to construct them in-house. Another avenue to pursue would be to assemble several heaters into larger banks. The 19- and 199-hexagon arrays would use a bank of two Watlow heaters side-by-side. This concept could be extended to include several more heaters and thereby enable the use of larger individual hexagons and fewer overall nodes.

We also chose particular configurations for deployment of the heaters (Figs. 3–6), and while these arrays should have good uniformity of the radiation distribution, these designs are not necessarily the best. Before any actual experiment is conducted on a particular ecosystem, the array configuration should be revisited to assure, for example, that the heights of the heaters above the vegetation are large with respect the height variation of the canopy top. If larger banks of heaters were assembled as suggested in the previous paragraph, heater heights would have to be adjusted to obtain optimal uniformity of the warming treatment across the plots.

The infrared heaters we considered are all electric (Table 1) largely because our previous experience utilized such electric heaters whose output could be modulated with commercially available dimmers in a PID control system (Kimball 2005; Kimball et al. 2008). However, other energy sources cost less than electricity (<http://www.eia.doe.gov/>). For the entire USA, the cost of natural gas on a per kWh basis is 39% of that for electricity. In Alaska, which is an area of interest due to large high-latitude

projected temperature increases and large stores of carbon locked into frozen soils, the average cost of natural gas is about 20% of that of electricity. Given these price differences, using natural gas instead of electricity could change the economics of a large warming experiment in Alaska from cost prohibitive to feasible.

Design of the support structures and control systems necessary to deploy multiple infrared heaters over large plots and estimating the associated initial capital costs must be considered when designing large-scale warming experiments, but they are beyond the scope of this paper. The selection and design of the structural components will be dependent on the selected location and ecosystem to be studied. The use of a control system that can independently control groups of heaters within the plot versus using a single control signal for all heaters should provide better spatial temperature control through better matching of the heater output to within plot variability. The cost/benefit calculations for adding the control circuitry and software necessary to obtain sub-plot level thermal control will need to be evaluated for each experiment, and the answer will depend on local environmental conditions and available funds. This fine-scale evaluation should be conducted during the testing of prototype designs, as was done with early Free Air CO<sub>2</sub> Enrichment designs for low stature (Hendrey et al. 1992) and forest (Hendrey et al. 1999) ecosystems. The capital construction costs will also depend greatly on the infrastructure for power and other resources already available at the selected location. Generally, however, we would expect these initial costs to be on the same order as 1 year's operating costs.

## 7 Conclusions

1. The distribution of thermal radiation and its uniformity from several commercially available infrared heaters with near black body emitting surfaces can be computed from theoretically derived angle factors.
2. The radiation from a single heater is cone shaped, so only a relatively small plot area will receive a uniform warming treatment. In contrast, by moving to large plots with arrays of heaters arranged in hexagons, excellent uniformity can be achieved. Likewise, by adjusting heater heights and spacing, good uniformity can also be achieved with rectangular plots.
3. The radiometric efficiency of an infrared heater is the fraction of electrical power input that results in thermal radiation output, and at zero wind, it appears to be about 85% to 90% for commercially available infrared heaters. In contrast, as wind speed increases, the efficiency of smaller heaters decreases more than that of larger heaters, such that at a wind speed of 4 m s<sup>-1</sup>, the radiometric efficiency of a 152-mm Watlow heater is about 56% compared to about 80% for a 1,016-mm heater.
4. Geometric efficiency is the fraction of emitted thermal radiation that falls within a defined useable plot area. For small arrays on the scale of 1 m, this can be less than 10% compared to over 80% at the 100-m scale for a 199-hexagon honeycomb array.
5. Overall efficiency is the fraction of electrical power input that results in thermal radiation impinging on vegetation within the defined plot area, and it is the product of the radiometric and geometric efficiencies. For small arrays on the scale of 1 m, overall efficiency is about 6% or less, whereas for 100-m arrays, it should be in the 65–75% range depending on wind speed.
6. Single 250-W heaters, such as have been used in several experiments, lack the power to provide 4°C of warming under Bondeville, IL, USA conditions. In contrast, by combining multiples of more powerful heaters in hexagonal, honeycomb arrays, as well as rectangular arrays, it should be possible to achieve 4°C of warming 85–98% of the growing season daytime hours. At night, with the stomata closed and calmer winds, these same arrays should be able to provide such warming almost all the time.
7. Under Bondeville, IL, USA conditions, assuming no water stress (ET is maximal) and dormancy (no ET) when temperatures are below freezing for a vegetation canopy with the characteristics of alfalfa, annual electrical power requirements for 4°C of warming would amount to about 15, 68, 250, 1,300, and 23,000 MWh per plot for 1-, 3-, 8-, 20-, and 100-m-diameter plots, respectively, using arrays with unlimited capacity. The amounts for 2×2-, 7.1×7.1-, and 2×20-m plots would be 44, 290, and 240 MWh per plot, respectively. For 7-m-tall trees in the 100-m-diameter plots, the requirements would be about 3.5 times greater than for 0.5-m alfalfa.
8. On a unit area basis, the annual power requirements amount to about 60,000, 9,600, 4,900, 4,000, and 2,900 kWh m<sup>-2</sup> for the 1-, 3-, 8-, 20-, and 100-m-diameter plots, respectively, which shows an economy of scale.
9. For electrical energy prices at US\$0.1/kWh, the annual energy costs would be about US\$1,500, US\$6,800, US\$11,000, US\$130,000, and US\$2,300,000 per plot for the 1-, 3-, 8-, 20-, and 100-m-diameter plots, respectively. On a unit area basis, the annual costs would be US\$6,000, US\$960, US\$490, US\$400, and US\$290 m<sup>-2</sup>, again showing an economy of scale.
10. If vegetation of progressively larger stature is grown in the progressively larger plots, the consequent decrease in aerodynamic resistance associated with

taller plant height would largely negate the improvements in efficiency compared to 3-m plots.

11. Solar shading should generally be less than 6% for the larger arrays.

**Acknowledgements** We appreciate the sharing of Bondeville, IL weather data by Andy VanLooche from the Department of Atmospheric Sciences, University of Illinois, Urbana, IL, USA. This research was supported by the US Department of Agriculture, Agricultural Research Service and by the U.S. Department of Energy (DOE), Office of Science, Biological and Environmental Research (BER) program and by the US Department of Energy Office of Science contract No. DE-AC02-98CH10886 to Brookhaven National Laboratory. USDA and DOE are equal opportunity providers and employers.

## References

- Ainsworth EA, Beier C, Calfapietra C, Ceulemans R, Durand-Tardif M, Farquhar GD, Godbold DL, Hendrey GR, Hickler T, Kaduk J, Karnosky DF, Kimball BA, Körner C, Koornneef M, LaFarge T, Leakey ADB, Lewin KF, Long SP, Manderscheid RM, McNeil DL, Mies TA, Miglietta F, Morgan JA, Nagy J, Norby RJ, Norton RM, Percy KE, Rogers A, Soussana J-F, Stitt M, Weigel H-J, White JW (2008) Next generation of elevated [CO<sub>2</sub>] experiments with crops: a critical investment for feeding the future world. *Plant Cell Environ* 31:1317–1324
- Allen RG, Walter IA, Elliott RL, Howell TA, Itenfisu D, Jensen ME, Snyder RL (2005) The ASCE standardized reference evapotranspiration equation. American Society of Civil Engineers, Reston
- Bijoor NS, Czimezik CI, Pataki DE, Billings SA (2008) Effects of temperature and fertilization on nitrogen cycling and community composition of an urban lawn. *Global Change Biol* 14:2119–2131
- Campbell GS (1977) An introduction to environmental biophysics. Springer, New York
- Gebhart B (1961) Heat transfer. McGraw-Hill, New York
- Ham JM (2005) Useful equations and tables in micrometeorology. In: Hatfield JL, Baker JM (eds) *Micrometeorology in Agricultural Systems*. American Society of Agronomy, Crop Science Society of Agronomy, and Soil Science Society of America, Madison, pp 533–560
- Harte J, Torn MS, Chang F-R, Feifarek B, Kinzig A, Shaw R, Shen K (1995) Global warming and soil microclimate results from a meadow-warming experiment. *Ecol Appl* 5:132–150
- Hendrey GR (1993) Free-air carbon dioxide enrichment for plant research in the field. Smoley, Boca Raton
- Hendrey GR, Lewin KF, Kolber Z, Evans LS (1992) Controlled enrichment system for experimental fumigation of plants in the field with sulfur dioxide. *J Air Waste Manag Assoc* 42:1324–1327
- Hendrey GR, Ellsworth DS, Lewin K, Nagy J (1999) A Free-Air CO<sub>2</sub> Enrichment System (FACE) for exposing tall forest vegetation to elevated atmospheric CO<sub>2</sub>. *Global Change Biol* 5:293–309
- Hovenden MJ, Miglietta F, Zaldei A, Vander Schoor JK, Wills KE, Newton PCD (2006) The TASFACE climate-change impacts experiment: design and performance of combined CO<sub>2</sub> and temperature enhancement in a native Tasmanian grassland. *Aust J Bot* 54:1–10
- Howell JR (2001) A catalog of radiation heat transfer configuration factors, 2nd edition. <http://www.me.utexas.edu/~howell/>
- Kimball BA (2005) Theory and performance of an infrared heater for ecosystem warming. *Global Change Biol* 11:2041–2056
- Kimball BA (2011) Comment on the comment by Amthor et al. on “Appropriate experimental ecosystem warming methods” by Aronson and McNulty. *Agr Forest Meteorol* 151:420–424
- Kimball BA, Conley MM (2009) Infrared heater arrays for warming field plots scaled up to five meters diameter. *Agr Forest Meteorol* 149:721–724
- Kimball BA, Conley MM, Wang S, Lin X, Luo C, Morgan J, Smith D (2008) Infrared heater arrays for warming ecosystem field plots. *Global Change Biol* 14:309–320
- Körner C, Asshoff R, Bignucolo O, Hättenschwiler S, Keel SG, Peláez-Riedl S, Pepin S, Siegwolf RTW, Zotz G (2005) Carbon flux and growth in mature deciduous forest trees exposed to elevated CO<sub>2</sub>. *Science* 309:1360–1362
- Lewin KF, Nagy J, Nettles WR, Cooley DM, Rogers A (2009) Comparison of gas use efficiency and treatment uniformity in a forest ecosystem exposed to elevated [CO<sub>2</sub>] using pure and prediluted free-air CO<sub>2</sub> enrichment technology. *Global Change Biol* 15:388–395
- Luo C, Xu G, Chao Z, Wang S, Lin X, Hu Y, Zhang Z, Duan J, Cang X, Su A, Li Y, Zhao X, Du M, Tang Y, Kimball B (2010) Effect of warming and grazing on litter mass loss and temperature sensitivity of litter and dung mass loss on the Tibetan plateau. *Global Change Biol* 16:1606–1617
- Mahrt L, Ek M (1984) The influence of atmospheric stability on potential evapotranspiration. *J Clim Appl Meteorol* 23:222–234
- Miglietta F, Zaldei A, Peressotti A (2001) Free-air CO<sub>2</sub> enrichment (FACE) of a poplar plantation: the POPFACE fumigation system. *New Phytol* 150:465–476
- Monteith JL (1973) Principles of environmental physics. Edward Arnold, London
- Nijs I, Kockelbergh F, Teughels H, Blum H, Hendrey G, Impens I (1996) Free air temperature increase (FATI): a new tool to study global warming effects on plants in the field. *Plant Cell Environ* 19:495–502
- Okada M, Lieffering M, Nakamura M, Yoshimoto M, Kim M, Kobayashi K (2001) Free-air CO<sub>2</sub> enrichment (FACE) using pure CO<sub>2</sub> injection: system description. *New Phytol* 150:251–260
- VanLooche A, Bernacchi C, Twines TE (2010) The impacts of *Miscanthus x giganteus* production on the Midwest US hydrologic cycle. *GCB Bioenergy* 2:180–191
- Wall GW, Kimball BA, White JW, Ottman MJ (2011) Gas exchange and water relations of spring wheat under full-season infrared warming. *Global Change Biol* 17:2113–2133